31st Annual International Conference of the IEEE EMBS
Minneapolis, Minnesota, USA, September 2-6, 2009

Nonlinear, data-driven modeling of cardiorespiratory control mechanisms

Georgios D. Mitsis, *Member, IEEE*

Abstract — **We present applications of recently developed algorithms for data-driven nonlinear systems identification to the study of cardiovascular and respiratory control mechanisms on an integrated systems level, utilizing experimental data obtained during resting conditions. Specifically, we consider cerebrovascular regulation during normal conditions, orthostatic stress and autonomic blockade in a two-input context, as well as respiratory control during a model opioid drug (remifentanil) infusion in a closed-loop context. The results illustrate the potential of using data-driven modeling approaches, which do not rely on prior assumptions about model structure, for modeling physiological systems, as they are well-suited to their complexity. They also illustrate the potential of utilizing spontaneous physiological variability, which can be monitored noninvasively and does not require experimental interventions, to extract rich information about the function of the underlying mechanisms. We also discuss some important practical issues, such as the presence of nonstationarities and model order selection, related to the application of similar approaches to the analysis of physiological systems.**

I. Introduction

Homeostasis, which describes the ability of living organisms to maintain themselves in a state of dynamic balance, is maintained by the complex interaction of multiple mechanisms, which typically involve feedback and nested loops and are often characterized by inherent nonlinearities. As a result of these mechanisms and their constant interaction with a fluctuating environment, stochastic variations over a wide range of time scales arise in physiological signals. Consequently, resting (spontaneous) physiological variability, which can be nowadays monitored continuously and noninvasively, contains rich information about the function of the underlying mechanisms under natural operating conditions, i.e., without any experimental intervention. Hence, it has been used extensively for their study, along with various signal processing and mathematical modeling/ systems identification techniques, opening up a host of potential patient-customized diagnostic and therapeutic applications (e.g. model-based physiological control) applications.

In this context, cardiovascular and respiratory control mechanisms are of particular importance as they regulate variables such as blood pressure and flow, heart rate and ventilation, which are crucial for the operation of the human organism. In the present paper we showcase the application of utilizing spontaneous physiological variability and recently developed nonlinear, data-driven systems identification approaches to the investigation of these mechanisms on an integrated systems level. Specifically, we consider cerebrovascular regulation under normal and various experimental conditions in a two-input context, as well as the investigation of the effects of opioid drugs on respiratory control in a closed-loop context.

The cerebrovascular bed is controlled by multiple homeostatic mechanisms (myogenic, endothelial, neural etc.) which are able to maintain cerebral blood flow (CBF) relatively constant despite changes in cerebral perfusion pressure [1]. Cerebral autoregulation was long viewed as a static phenomenon, whereby the "steady-state" pressure-flow relationship is described by a sigmoidal curve with a wide plateau, suggesting that CBF remains constant despite changes in pressure within certain bounds. However, with the development of Transcranial Doppler (TCD) ultrasonography for the noninvasive measurement of CBF velocity (CBFV), in the middle cerebral artery with high temporal resolution, it was found that spontaneous CBFV variations, may vary rapidly in response to variations of systemic arterial blood pressure (ABP) over various time scales [2]. Furthermore, the cerebrovascular bed is exquisitely sensitive to changes in arterial CO_2 [1]. Spontaneous fluctuations of arterial CO_2 tension around the mean, assessed by end-tidal CO_2 (P_{ETCO2}) measurements, have a significant effect on slow fluctuations of both CBFV as well as regional blood flow, assessed by blood oxygen dependent level functional magnetic resonance imaging [3], [4]. It has also been suggested that cerebral hemodynamics are characterized by nonlinearities, both on the basis of the low coherence values between ABP and MCBFV below 0.07 Hz [2] and by exploring the use of nonlinear Volterra models [5]. Therefore, we have introduced a two-input, nonlinear model of cerebral hemodynamics [6], shown in Fig. 1, and in the present paper we show results obtained from utilizing this model to study cerebrovascular regulation during normal conditions, orthostatic stress and autonomic blockade.

Much of the understanding of human respiratory control is based upon characterization of the ventilatory feedback loop, which is shown in Fig. 2 in a simplified form, supplemented by inferences from work in animals. Ventilatory responses are usually examined during hypoxic or hypercapnic stimulation [7]. Moreover, it has been shown that spontaneous breath-to-breath fluctuations in P_{ETCO2} are responsible for a considerable fraction of the normal

Manuscript received April 23, 2009.

Georgios D Mitsis is with the Department of Electrical and Computer Engineering, University of Cyprus, Nicosia 1678, Cyprus (e-mail: gmitsis@ucy.ac.cy).

variability in tidal volume (V_T) [8], and the dynamic effects of these spontaneous fluctuations have been used to derive information on ventilatory feedback [9]. Respiratory depression is the most common serious side effect of opioid drugs, as these drugs lead to slowing and increasing irregularity of the respiratory rhythm by depressing chemosensitive and rhythm generating centers in the brainstem [10], [11]; therefore, avoiding respiratory depression remains an important clinical aim.

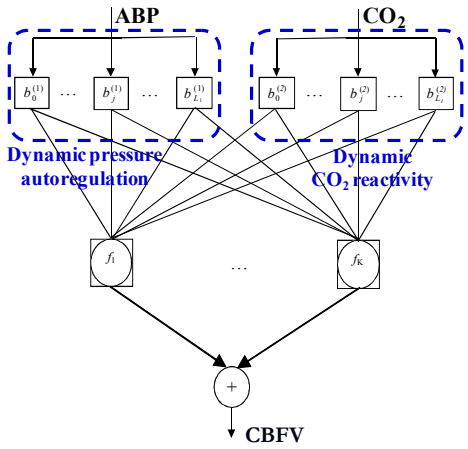

Fig. 1. Two-input, nonlinear model of cerebrovascular regulation, which includes the dynamic effects of ABP and arterial CO_2 (assessed by P_{ETCO2}) on CBFV, termed dynamic pressure autoregulation and CO_2 reactivity respectively.

In the present paper we also consider the effects of a model opioid drug used in analgesia and anaesthesia (remifentanil) infusion on respiratory control by quantifying the dynamic interrelationships between P_{ETCO2}, V_T and breath-to-breath ventilation (V_T/T_{TOT}, where T_{TOT} is total breath time) in both causal directions of the ventilatory loop. To this end, we use a nonlinear modeling approach (Laguerre expansion technique) to quantify the dynamic influence of spontaneous P_{ETCO2} fluctuations on ventilatory variability (the forward part of the ventilatory loop) and the influence of ventilatory variability on P_{ETCO2} (the reverse part of the loop).

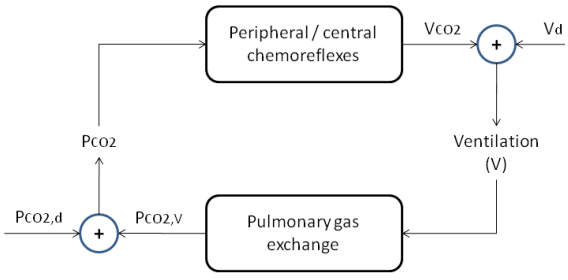

Fig. 2. Simplified diagram of the ventilatory feedback loop. Spontaneous ventilatory variability arises from a chemical component V_{CO2} that is due to variations in CO_2 variability P_{CO2}, and a non-chemical component V_d (disturbance) due to all other physiological influences. Similarly, spontaneous P_{CO2} variability arises from a ventilatory related component $P_{CO2,V}$ that is due to variations in V_T and a non-ventilatory related component $P_{CO2,d}$.

II. METHODS

The study of many important physiological systems has been pursued in the Volterra-Wiener framework [12]. According to this, the general Volterra model for a Q-th order nonlinear system with memory M in discrete time is:

$$y(n)=\sum_{q=0}^{Q}\sum_{m_1=0}^{M}\cdots\sum_{m_q=0}^{M}k_q(m_1,\ldots,m_q)x(n-m_1)\ldots x(n-m_q) \quad (1)$$

where $x(n)$ and $y(n)$ are the system input and output respectively, M is the system memory and $k_q(m_1,\ldots,m_q)$ are the Volterra kernels of the system, which describe the linear (Q=1) and nonlinear (Q>1) dynamic effects of the input on the output. Eq. (1) reduces to the convolution sum for linear systems (Q=1), with $k_1(m)$ corresponding to the impulse response of the system.

Among various methods that have been developed for the estimation of the discretized Volterra kernels from input-output data, the utilization of function expansions in terms of the orthonormal Laguerre basis has been proven to be particularly efficient [13]:

$$k_q(m_1,\ldots,m_q)=\sum_{j_1=0}^{L}\cdots\sum_{j_q=j_{q-1}+1}^{L}c_{j_1\ldots j_q}b_{j_1}(m_1)\ldots b_{j_q}(m_q) \quad (2)$$

where $c_{j1\ldots jn}$ are the expansion coefficients, $b_j(m)$ is the j-th order Laguerre function and L+1 is the total number of functions that yields an adequate system representation. In matrix form:

$$\mathbf{y}=\mathbf{V}\mathbf{c}+\boldsymbol{\varepsilon} \quad (3)$$

where $\mathbf{V}$ is a matrix that contains the convolution of $x(n)$ with the Laguerre functions $\{b_j\}$ and their second (or higher) order products. The expansion coefficients can be obtained as the least-squares solution of (3) [13]:

$$\mathbf{c}_{est}=[\mathbf{V}^T\mathbf{V}]^{-1}\mathbf{V}^T\mathbf{y} \quad (4)$$

We used this approach in order to quantify the effects of remifentanil on respiratory control in both directions of the ventilatory loop (Fig. 2). For the chemoreflex pathway ($P_{ET}CO_2 \rightarrow V$) sighs, which were defined as breaths with values greater than 1.5 times the mean breath value were removed by linear interpolation before model estimation, as they are viewed as part of the disturbance component of V (V_d in Fig. 1). Furthermore, a pure time delay of 2 breaths was hypothesized in the effects of P_{ETCO2}.

The experimental data were collected from 11 healthy volunteers (age 27±5years) during resting conditions (normal breathing) and remifentanil infusions of zero (baseline), 0.7, 1.1 and 1.5 ng/ml. The target-controlled infusion of remifentanil was delivered via an indwelling intravenous cannula inserted into a vein in the left forearm. Oxygen saturations, heart rate, $P_{ET}CO_2$ and $P_{ET}O_2$ were monitored continuously using a Datex Cardiocap II, while respiratory volume and timing was measured with a turbine respiratory flow meter (VMM-400, Interface Associates). The baseline recordings were taken for 15 minutes. For each level of remifentanil, five minutes were allowed to reach target effect site concentration; continuous recordings were made for the following 15 minutes at that stable effect site concentration.

In the case of cerebrovascular regulation, we utilized a Volterra-equivalent network termed the Laguerre-Volterra Network (LVN) to obtain the system Volterra kernels (Fig. 1). The LVN methodology combines Laguerre function expansions and networks with polynomial activation functions and has been shown to yield accurate models of high-order and multiple-input systems from short input-output records [6], [14]. In this context, the output of the two-input mode of cerebrovascular regulation of Fig. 1 in terms of the MABP and P_{ETCO2} inputs is given by:

$$CBFV(n) = k_0 + \sum_{i=1}^{2}\sum_{m_1} k_{1x_i}(m_1)x_i(n-m_1) + \\ + \sum_{i_1=1}^{2}\sum_{i_2=1}^{2}\left\{\sum_{m_1}\sum_{m_2} k_{2x_{i_1}x_{i_2}}(m_1,m_2)x_{i_1}(n-m_1)x_{i_2}(n-m_2)\right\} + \ldots \quad (5)$$

where x_i: MABP, P_{ETCO2}. The linear and nonlinear Volterra kernels k_q describe the linear and nonlinear effects of MABP and P_{ETCO2} (as well as their nonlinear interactions) at time lags (m_1,...,m_q) before the present time lag n on CBFV and are used to quantify dynamic pressure autoregulation and CO_2 reactivity respectively. The Volterra kernels in (5) can be expressed in terms of the LVN parameters, which are in turn estimated via an iterative gradient descent algorithm from the input-output data. Therefore, dynamic pressure autoregulation and dynamic CO_2 reactivity are described by $k_{qxi...xi}$ for i=1 and i=2 respectively.

In all the experimental protocols considered herein, P_{ETCO2} was measured by mass spectrometry, ABP was monitored continuously in the finger by photoplethysmography and CBFV was measured with a 2-MHz Doppler ultrasound system in the right middle cerebral artery. The beat-to-beat values of ABP and CBFV and the breath-to-breath values of P_{ETCO2} were interpolated and resampled at 1 Hz to obtain equally spaced time series. Model estimation was performed using 6 min segments.

The experimental data during resting conditions (total 40 mins) were collected from 10 healthy subjects (age 30.4± 20.1 years). The experimental data during orthostatic stress were collected from 10 healthy subjects (age 32.1±7.3 years), whereby orthostatic stress was induced by graded lower body negative pressure (LBNP) after at least a 30-min baseline period according to the following protocol: -15 mmHg and -30 mmHg for 13 min, and then progressively by -10 mmHg every 13 min to the point of maximal tolerance. Finally, experimental data during autonomic blockade were recorded from 12 healthy subjects (age 29±6 years). Trimethaphan, which induces ganglionic blockade, was infused at a dose of 3 mg/min. Blockade was assessed by evaluating both the heart rate and pressure responses to the Valsalva maneuver. The infusion dose was increased incrementally by 1 mg/min until the heart rate response during the Valsalva maneuver was eliminated. Since the low-frequency ABP variability after ganglion blockade was reduced, oscillatory lower body negative pressure (LBNP) with a magnitude of 0 to -5 mmHg was applied in 10 subjects.

We used the normalized mean-square error (NMSE) of the output prediction to assess model performance and determine model complexity in all cases. This was done by utilizing statistical criteria to assess the significance of the NMSE reduction achieved by more complex models, such as the minimum description length criterion and by comparing the percentage NMSE reduction to the α-percentile value of a χ^2 distribution with p degrees of freedom (where p is the increase of the number of free parameters and α=0.05).

III. Results

A. Cerebrovascular regulation

The average achieved prediction NMSEs are given in Table I for one input (ABP or P_{ETCO2}) and two-input (ABP and P_{ETCO2}) linear and nonlinear LVN models in the case of resting conditions. ABP fluctuations explain most of the CBFV variations; however, the incorporation of P_{ETCO2} in the model reduces the achieved output prediction NMSEs. A significant reduction in the prediction NMSE is also observed when nonlinear models are used [6]. Hence, the previously reported low coherence values between ABP and CBFV below 0.07 Hz are due to the effect of both nonlinearities and CO_2 fluctuations. This is further illustrated in Fig. 3, where we show the decomposition of the model prediction for a representative data segment into its linear and nonlinear components, as well as into its ABP and CO_2 components [6]. Examination of the model residuals in the frequency domain (Fig. 3 – right panels) reveals that the contribution of these terms, which corresponds to the area between the blue and red lines, is more pronounced below 0.05 Hz.

The first-order ABP and CO_2 kernels, averaged over all subjects, are shown in the time and frequency domains in Fig. 4. The high-pass characteristic of the linear ABP frequency response implies that slow MABP changes are attenuated more effectively, i.e., autoregulation of pressure variations is more effective below 0.07 Hz. The tight standard error bounds imply that the form of the linear ABP kernel was consistent across subjects. The linear first-order CO_2 kernel exhibits a low-pass characteristic rather than the high-pass characteristic of its MABP counterpart. Typical second-order MABP and CO_2 kernels are shown in Fig. 5. Most of the power of the second-order kernels lies below 0.1 Hz. The second-order kernels were more variable compared to the linear kernels. Moreover, their frequency domain peaks were related to their linear counterparts.

TABLE I
CEREBROVASCULAR REGULATION DURING RESTING CONDITIONS: PREDICTION NMSES (MEAN±SD) FOR ONE-INPUT AND TWO-INPUT MODELS.

Model order	Model inputs [NMSE in %]		
	ABP	P_{ETCO2}	ABP & P_{ETCO2}
1	42.2 ±7.2	93.2±2.7	38.2±6.5
2	25.7± 8.3	78.2±25.7	22.0 ± 6.0
3	26.8±7.6	71.7±4.8	20.2±5.4

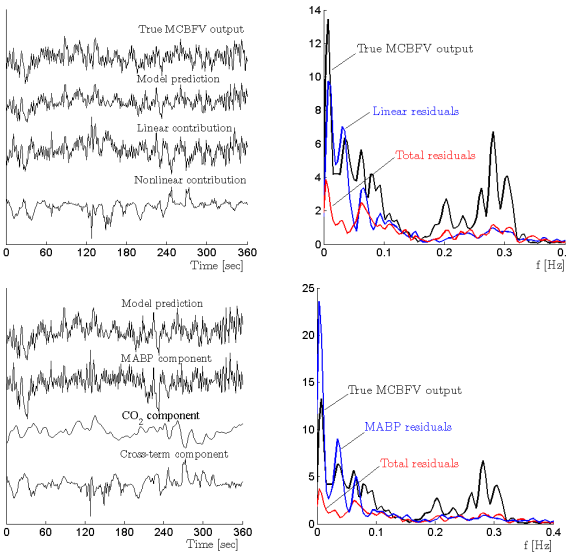

Fig. 3. Decomposition of model prediction of the two-input nonlinear model of cerebrovascular regulation into linear and nonlinear components, as well as into ABP and CO_2 components, for a representative data segment in the time (left) and frequency (right) domains - resting conditions.

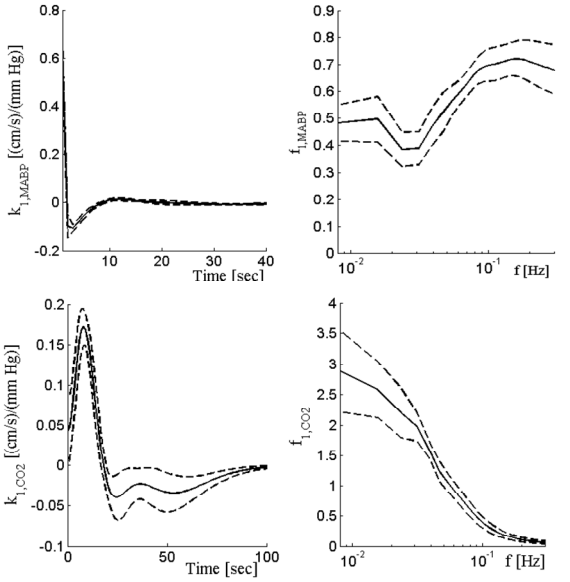

Fig. 4. First-order MABP and CO_2 kernels (solid lines) and corresponding standard errors (dotted lines), averaged over all subjects – resting conditions. Left panel: time domain, right panel: FFT magnitude.

The first-order kernels obtained during orthostatic stress (baseline to -50 mm Hg LBNP) are shown in Fig. 6 [15]. The magnitude of the ABP kernel in the very low frequency (VLF) range (f<0.04 Hz) increased gradually during LBNP, whereas the magnitude in the low frequency (LF; 0 .04<f<0.15 Hz) and high frequency (HF; 0.15<f<0.3 Hz) ranges remained relatively unchanged. Consequently, the high-pass characteristic of the ABP linear frequency response at baseline was gradually altered to a band-stop characteristic at high levels of LBNP values. The CO_2 kernel exhibited a low-pass characteristic that was not altered during LBNP; however, its magnitude values decreased with increasing LBNP (results not shown, see [15]).

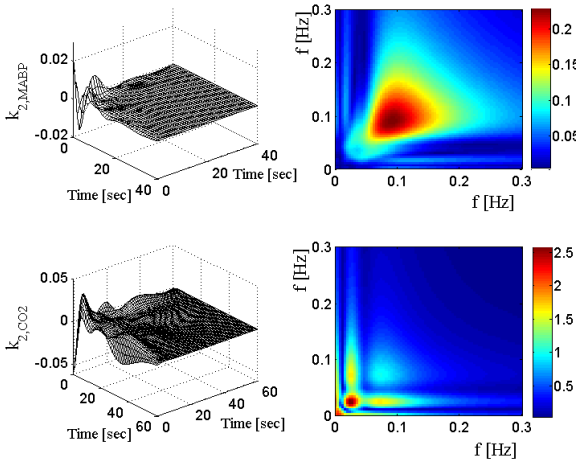

Fig. 5. Representative second-order MABP and CO_2 kernels. Left panel: time domain, right panel: 2D-FFT magnitude.

Similar effects of orthostatic stress on the second-order ABP and CO_2 kernels were observed. As a result, the spectral power of the ABP first and second-order components, which was calculated in the VLF, LF and HF ranges by integrating the corresponding frequency responses between the respective frequency limits, increased during LBNP (P<0.05 at -40 and -50 mm Hg for the VLF range). On the other hand, the spectral power of the CO_2 components decreased during LBNP (P<0.05 at -40 and -50 mm Hg LBNP in the VLF and LF ranges [15]).

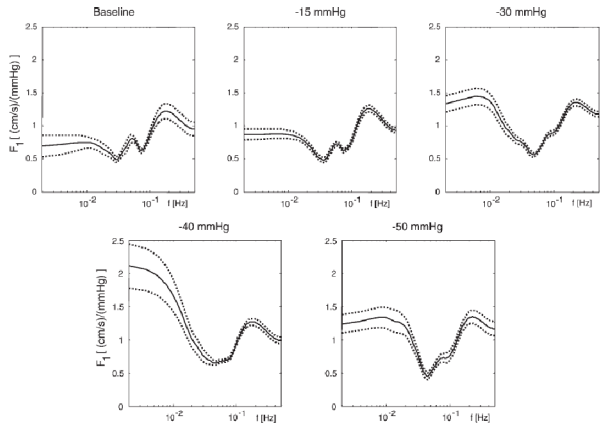

Fig. 6. Group-averaged first-order ABP kernels in the frequency domain (F_1) during baseline and LBNP-induced orthostatic stress (solid line: mean value, dotted line: SE). Note the increase in very-low-frequency (VLF, f<0.04 Hz) magnitude during LBNP.

The averaged first-order ABP kernel during baseline, ganglionic blockade and simultaneous blockade and LBNP is shown in Fig. 7 in the frequency domain (top panels). The high-pass characteristic during baseline was altered to a band-stop characteristic during ganglion blockade (both without and with simultaneous LBNP), as in the case of orthostatic stress, i.e. its magnitude increased in the VLF and LF ranges. The dynamic CO_2 reactivity linear component exhibited a low-pass characteristic during baseline and

ganglionic blockade (Figure 7, bottom panels), albeit with decreased magnitude during the latter. The second-order model components are shown in Fig. 8 in the frequency domain averaged over all subjects. Most of their power resides below 0.15 Hz and they were affected by ganglionic blockade similarly to their first-order components; the values of f_{2MABP} and f_{2CO2} increased and decreased respectively. The spectral power of k_{1MABP} increased significantly in the VLF range (P<0.01) during ganglion blockade and in the VLF and LF ranges (P<0.05) during simultaneous blockade and LBNP. On the other hand, the differences in the linear CO_2 kernel spectral power were marginally significant, mainly due to the more pronounced variability of the individual estimates. The second-order components exhibited similar trends with the differences being marginally significant in the LF range for the MABP and P_{ETCO2} components between baseline and ganglion blockade (without LBNP).

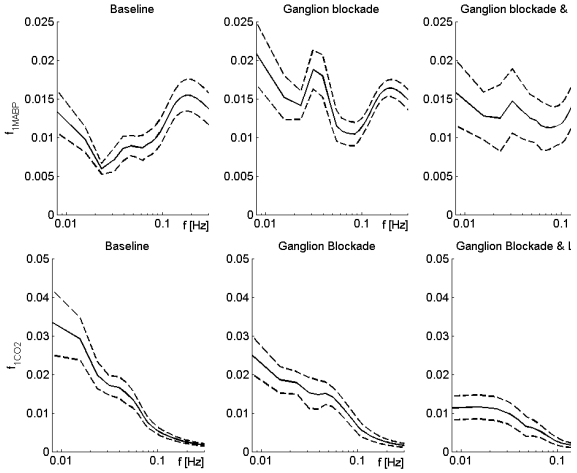

Fig. 7. Linear component of dynamic pressure autoregulation (top panels) and CO_2 reactivity (bottom panels) during baseline and ganglionic blockade in the frequency domain, averaged over all subjects (Mean±SE). The magnitude of f_{1MABP} in the VLF and LF ranges (below 0.15 Hz) increased during ganglion blockade.

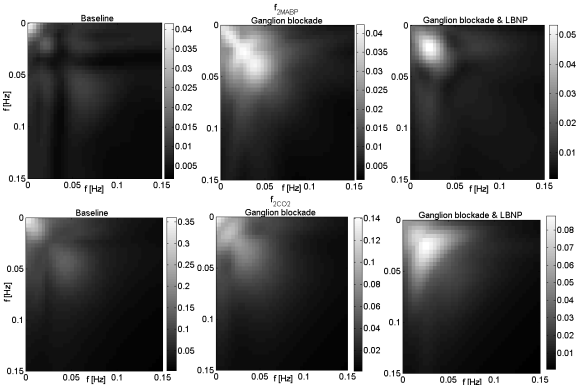

Fig. 8. Second-order component of dynamic pressure autoregulation (top panels) and CO_2 reactivity (bottom panels) in the frequency domain (2D FFT) during baseline and ganglionic blockade, averaged over all subjects.

B. Respiratory control during opioid infusion

The effects of remifentanil on the respiratory variables were: (i) a dose-dependent decrease in respiratory rate that was due to increases in duration of expiratory time (TE) and its variability coefficient (results not shown, see [16]) (ii) V_T initially decreased (at 0.7 ng/ml) but increased at higher levels towards baseline values and (iii) $PETCO_2$ increased and became more variable. The spectral power of P_{ETCO2} and V_T was calculated by integrating their PSD functions from 0 to 0.3 cycles/ breath. An increase over the entire frequency range was observed for $PETCO_2$. V_T spectral power increased during remifentanil infusion, albeit less pronouncedly and above 0.02 cycles/ breath [16]. Nonlinear models reduced the prediction NMSEs significantly in all cases and in both directions of the ventilatory loop [16]. Representative linear and nonlinear model predictions are shown in Fig. 9. P_{ETCO2} variations mainly account for the V_T post-sigh response, as sighs are clearly correlated with sharp $PETCO_2$ drops (as expected), which in turn influence V_T. These sharp drops are evidently accounted by the $V_T \rightarrow PETCO_2$ model. In the frequency domain, the incorporation of nonlinear model terms improved performance over a wide range of frequencies below 0.03 cycles/breath.

The averaged first-order kernels for the forward part of the ventilatory loop are displayed in Fig. 10, when both V_T (blue) and V_T/T_{TOT} (black) were used to assess ventilatory variability. Their form during baseline suggests that an increase in P_{ETCO2}will cause an increase in V_T (or V_T/T_{TOT}), with the maximum instantaneous effects occurring at 4 and 8 breaths after the P_{ETCO2} increase. The kernel values decreased during remifentanil, with the decrease being more evident for the second peak. An undershoot at 13 breaths was observed during baseline only. For the reverse branch of the ventilatory loop ($V \rightarrow PETCO_2$), the form of the first-order kernel suggests that an increase in ventilation will lead to a decrease in P_{ETCO2}, with the effects occurring almost instantaneously, i.e., within the first 2 breaths (results not shown). Remifentanil infusion did not alter these characteristics; however, the kernel values increased at all levels, suggesting a stronger dynamic effect of ventilatory variability on P_{ETCO2}.

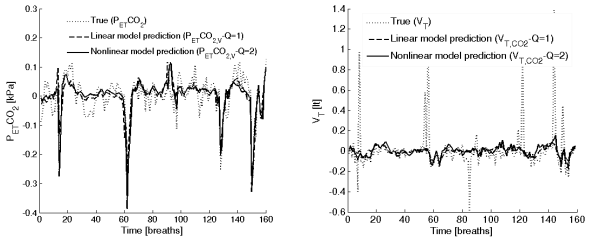

Fig. 9. P_{ETCO2} (left panel - dotted line) and V_T (right panel - dotted line) time series during baseline, used for model estimation in both pathways of the ventilatory loop, and corresponding nonlinear model predictions ($P_{ETCO2,V}$ and $V_{T,CO2}$ respectively, solid lines). The large drops in P_{ETCO2} induced by deep breaths (sighs) are clearly accounted by the $V_T \rightarrow P_{ETCO2}$ model (left - solid line), while P_{ETCO2} changes account mainly for the post-sigh V_T response (right – solid line).

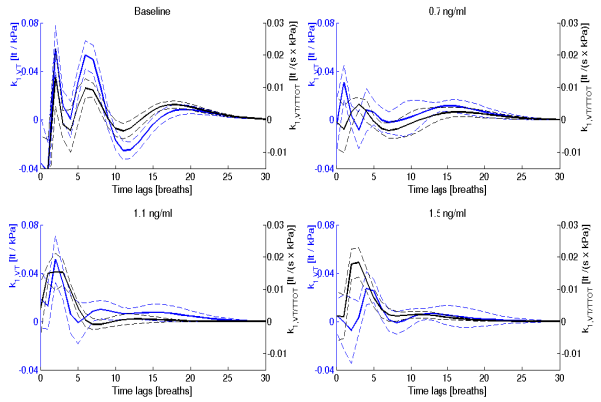

Fig. 10. Averaged first-order kernels for the chemoreflex pathway, whereby both VT (blue) and VT/TTOT (black) were used to assess ventilatory variability. Remifentanil decreased the impulse response values, particularly of the second peak. A secondary positive peak was also observed between 15 and 20 breaths.

The above observations are quantified by the spectral power of the first- and second-order kernels for both pathways shown in Fig. 11. For the chemoreflex branch (left), a decrease was observed in the spectral power of k_1 and k_2. This decrease was statistically significant only during the lowest level of remifentanil infusion for V_T; however, more pronounced differences were observed when V_T/T_{TOT} was used as the model output. For the reverse pathway (right), the k_1 spectral power increased significantly (P<0.01 during all remifentanil levels for V_T). The spectral power of the second-order model components k_2 increased as well (P<0.05 at 0.7 ng/ml).

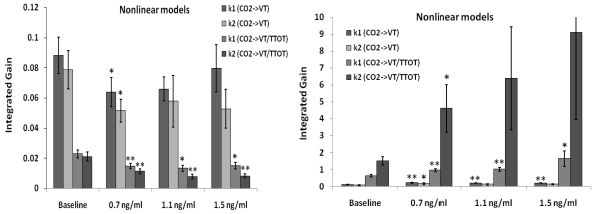

Fig. 11. Spectral power of the first and second-order Volterra kernels for the chemoreflex (left) and reverse (right) pathways. The spectral power of both the linear and nonlinear chemoreflex components between 0 and 0.3 cycles/ breath decreased during remifentanil infusion. * P<0.05, ** P<0.01 compared to baseline.

IV. Discussion

The presented results illustrate the potential of utilizing data-driven nonlinear modeling approaches to the study of cardiorespiratory regulatory mechanisms and, in a more general context, physiological systems on an integrated level. They also suggest that rich information regarding system function can be extracted from spontaneous physiological variability, which does not require any experimental interventions and can be often readily measured in real life clinical situations. This approach, as shown in the cases considered above whereby the effect of experimental and pharmacological interventions on the system characteristics was studied, can also assess changes induced by such interventions, providing information about the contribution of different mechanisms that are involved (e.g., neural mechanisms in the case of cerebrovascular regulation). Consequently, our knowledge about system function during normal and pathophysiological conditions may be further enhanced and such approaches may be applied to diagnostic and therapeutic purposes.

Since physiological mechanisms are typically affected by a large number of variables, it is important to incorporate as much information as possible, as shown above in the case of cerebrovascular regulation, whereby the incorporation of CO_2 as an input variable yielded more accurate descriptions of the system dynamics, particularly in the very low frequency range.

An issue that deserves further discussion is the presence of nonstationarity (time-varying behavior) in physiological systems, since it attains great significance in adaptive, real-time applications. These systems exhibit inherent nonstationarities, high complexity and are influenced by a large number of variables, some of which may often be unobservable in practice. Note that these factors may span widely different time scales: from local, fast acting mechanisms to circadian rhythms. Moreover, their influence may give rise to nonstationarities in the obtained models. An example of this situation was observed in cerebrovascular regulation, whereby the incorporation of arterial CO_2 variability as an additional determinant reduced the nonstationary behavior of the dynamic relationship between ABP and CBFV. The time-varying characteristics of the first-order cerebrovascular system dynamics, as obtained from the two-input model of Fig. 1 by tracking their evolution over the entire 40 min record for one representative subject and for sliding 6 min segments for a 5 min overlap, are shown in the time-frequency plot of Fig. 12. The ABP first-order kernel is more consistent (i.e. more stationary) than its CO_2 counterpart; also, more nonstationarities are observed in the lower frequency range.

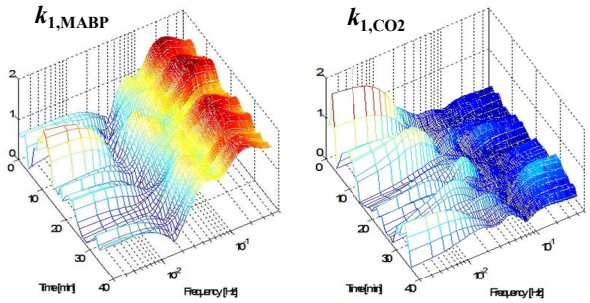

Fig. 12. Time-varying characteristics of the first-order cerebrovascular system ABP and CO_2 dynamics.

Finally, another issue of great importance is model order selection. This is usually achieved by using statistical criteria, such as the Akaike or the minimum description length criteria; however, these are not specifically designed for nonlinear systems and may yield biased results. Utilizing out-of-sample data for this purpose may also pose problems in cases where the amount of data is limited and/or when significant nonstationarities are present in the system dynamics. We are currently investigating the application of the Bayesian methods to perform model order selection for

nonlinear systems, specifically in the case of Laguerre function expansions [17].

ACKNOWLEDGMENT

The author would like to thank Prof. Vasilis Marmarelis, as well as Profs. Marc Poulin, Peter Robbins, Rong Zhang Benjamin Levine and Dr. Kyle Pattinson for providing the experimental data presented herein.

REFERENCES

[1] L. Edvinsson and D.N. Krause, *Cerebral Blood Flow and Metabolism*. Philadelphia, PA: Lippincott Williams and Wilkins, 2002.

[2] R. Zhang,, J.H. Zuckerman and B.D. Levine, "Spontaneous fluctuations in cerebral blood flow velocity: insights from extended duration recordings in humans," *Am. J. Physiol. 278* (*Heart Circ. Physiol.)*: H1848-1855, 2000.

[3] Panerai, R.B., Simpson, D.M, Deverson, S.T., Mahony, P, Hayes, P and D.H. Evans, "Multivariate dynamic analysis of cerebral blood flow regulation in humans," *IEEE Trans. Biomed. Eng.* vol. 47, pp. 419-421, 2000.

[4] R. G. Wise, K. Ide, M. J. Poulin, and I. Tracey, "Resting fluctuations in arterial carbon dioxide induce significant low frequency variations in BOLD signal," *Neuroimage,* vol. 21, pp. 1652-64, 2004.

[5] G. D. Mitsis, R. Zhang, B. D. Levine, and V. Z. Marmarelis, "Modeling of Nonlinear Physiological Systems with Fast and Slow Dynamics. II. Application to Cerebral Autoregulation," *Ann. Biomed. Engin.,* vol. 30, pp. 555-565, 2002.

[6] G. D. Mitsis, M. J. Poulin, P. A. Robbins, and V. Z. Marmarelis, "Nonlinear modeling of the dynamic effects of arterial pressure and CO_2 variations on cerebral blood flow in healthy humans," *IEEE Trans. Biomed. Eng.,* vol. 51, pp. 1932-1943, 2004.

[7] M.E. Pedersen, M. Fatemian and P.A. Robbins "Identification of fast and slow ventilatory responses to carbon dioxide under hypoxic and hyperoxic conditions in humans," *J Physiol* vol. 521, pp. 273-287, 1999.

[8] M. Modarreszadeh and E.N. Bruce "Ventilatory variability induced by spontaneous variations of PaCO2 in humans," *J Appl Physiol* vol. 76, pp. 2765-2775, 1994.

[9] J.G. van den Aardweg and J.M. Karemaker "Influence of chemoreflexes on respiratory variability in healthy subjects," *Am J Respir Crit Care Med* 165: 1041-1047, 2002.

[10] K.T. Pattinson **"**Opioids and the control of respiration," *Br J Anaesth* vol. 100, pp. 747-758, 2008.

[11] N.M. Mellen, W.A. Janczewski, C.M. Bocchiaro and J.L. Feldman "Opioid-induced quantal slowing reveals dual networks for respiratory rhythm generation," *Neuron* vol. 37, pp. 821-826, 2003.

[12] V. Z. Marmarelis, *Nonlinear Dynamic Modeling of Physiological Systems*. Piscataway, NJ: Wiley-Interscience & IEEE Press, 2004.

[13] V.Z. Marmarelis "Identification of nonlinear biological systems using Laguerre expansions of kernels," *Ann Biomed Eng* 21: 573-589, 1993.

[14] G.D. Mitsis and V.Z. Marmarelis, "Modeling of nonlinear systems with fast and slow dynamics. I. Methodology," *Ann. Biomed. Eng.*, vol. 30, pp. 272-281, 2002.

[15] G.D. Mitsis, R. Zhang, B. D. Levine, and V. Z. Marmarelis, "Cerebral hemodynamics during orthostatic stress assessed by nonlinear modeling," *J Appl Physiol,* vol. 101, pp. 354-66, 2006.

[16] G.D. Mitsis, R.J. Governo, R. Rogers and K.T. Pattinson, "The effect of remifentanil upon respiratory variability, evaluated with dynamic modeling," *J Appl Physiol,* vol. 106, pp. 1038-1049, 2009.

[17] G.D. Mitsis and S. Jbabdi, "Bayesian model order selection for nonlinear system function expansions," *Proc. 30th Ann. Conf. IEEE Engin. Med. Biol. Soc.,* Vancouver, BC, August 2008, pp. 2165-2168.